# ABLATION COMBUSTION OF SECONDARY POWDER EXPLOSIVES

**L. A. Luk'yanchikov, É. R. Pruuél, A. O. Kashkarov, and K. A. Ten**

UDC 536.46

*The explosive transformation in a passive charge initiated by an air shock wave was studied using synchrotron diagnostics of density. It was found that in the passive charge, a compression wave capable of forming effective hot spots does not arise and classical initiation conditions do not occur. The development of the reaction can be attributed to the ablation combustion observed in studies of the initiation of secondary powder explosives by a spark and gaseous detonation.*

**Key words:** *combustion, ablation combustion, detonation, synchrotron radiation.*

**Introduction.** In the first issue (1960) of the journal Applied Mechanics and Technical Physics was published a paper by A. F. Belyaev, M. A. Sadovskii, and I. I. Tamm "Application of the Similarity Law to Detonation Transmission in Explosions" [1], devoted to detonation transmission through air from active charges to passive charges consisting of secondary powder explosives of density 1 g/cm$^3$. It was found that in a passive charge of small diameter, detonation transformation developed in a low-strength shell within not more than 10 $\mu$sec after the arrival of the shock wave from the active charge at the explosive–air interface. It was shown that detonation transmission was determined by the maximum pressure arising on the interface. The initiation mechanism, which is of interest due to the weakness of the external action and the small time of its development, was not considered in [1]. Let us analyze the results of experiments [1], which are shown schematically in Fig. 1.

Bulk RDX, TNT, and ammonite of the same density 1 g/cm$^3$ were used as passive charges with no strong shell. The active charges were 50/50 TNT/RDX and RDX of density 1.43 and 1.10 g/cm$^3$, respectively. The weight of these charges ranged from 23 to 135 g. The spherical shape of the active charge made it possible to analyze the results of the experiments using similarity laws. In the calculations, the TNT equivalent of the charges was determined from the formula

$$C_e = C\varepsilon/\varepsilon_{\text{TNT}}.$$

Here $\varepsilon_{\text{TNT}}$ is the specific heat of explosion of TNT, $\varepsilon$ is the specific heat of explosion of the given explosive. For small charges, the weight of the active charge $C^*$ was determined in a special series of experiments taking into account that in such charges, part of the explosive scatters.

In the experiments, the distance between the charges $R_{50}$ providing 50% probability of detonation transmission was determined and optical photo recording was performed.

The initiating ability of the active charge was estimated using the normalized distance

$$R_{50}^* = C^*\varepsilon/(C_e^*)^{1/3}.$$

It was found that for a fixed passive charge, the normalized distance remains almost identical for all active charges used. From the similarity law, it follows that the same normalized distances $R_{50}^*$ correspond to the same maximum shock-wave pressures and parameters of the flow of explosion products in air as well as the same velocities of shock-wave propagation and expansion of the explosion products.
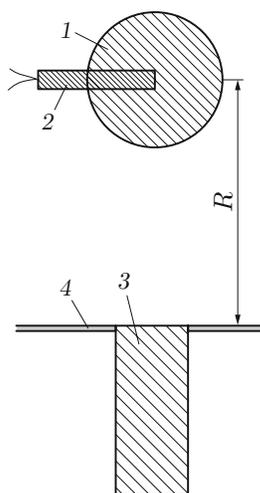
Fig. 1. Basic version of the experimental setup for detonation transmission used in [1]:
1) active charge; 2) detonator; 3) passive charge; 4) screen.

Analysis of the experimental and calculation results led to the following conclusions:

1. Detonation transmission depends on the pressure of the incident shock waves (in this case, in air). These shock waves have the following velocities: 2650 m/sec for RDX, 3850 m/sec for 50/50 TNT/RDX, and 4100 m/sec for ammonite.

2. The source of the initiating action is the region at the passive charge–air interface, at which the pressure produced by the reflected shock wave is 650 atm (65 MPa) for RDX, 1800 atm (0.18 GPa) for 50/50 TNT/RDX, and 4100 atm (0.41 GPa) for ammonite.

3. In a low-strength shell with a small charge diameter, detonation transformation is completed within no more than 10 $\mu$sec.

In [1], possible mechanisms of explosive transformation were not considered. Although more than 50 years passed since the publication, the full significance of the results obtained in [1] has not been evaluated up to now. This is due to a lack of sufficient experimental information on the transition process because of limited capabilities of standard recording procedures. The use of synchrotron radiation to determine the density dynamics during such initiation has made it possible to obtain additional experimental data [2–4]. Below, we give the results of experimental studies showing that, in this case, detonation propagation cannot be explained within the framework of the classical explosive-transition modes [5].

**1. Experimental Technique.** Synchrotron radiation (SR) (in the case considered, soft x-rays) arises from motion of electron beams on curvilinear trajectories in accelerators.

Unlike in classical sources, in which x-ray photons are produced when the electrons accelerated by an electric field are decelerated as a result of interaction with a metallic anode, SR has the following advantages:

1) high radiation intensity [$10^{16}$–$10^{21}$ photon/(sec · cm$^2$)];

2) small angular divergence ($\alpha = 10^{-3}$–$10^{-5}$ rad);

3) generation of radiation pulses following one after another at a stable frequency $f$ determined by the accelerator operation mode;

4) small length of radiation pulses (less than 1 nsec).

These properties of SR allow it to be used to measure material density during development and propagation of explosion processes. This was done using a high-intensity ray passing without deviation and providing information on the material density. In the experiments, a homogeneous ray 0.4 mm high and $H = 18$ mm wide was used.

Moving photons are recorded in measuring SR systems using radiation detectors with a large number of channels (usually more than 200) of width $h$. The response of the detector to an absorbed photon was a current pulse recorded by an electronic circuit over all channels. In the experiments performed, a DIMEX detector [6–8] having 250 channels with $h = 100$ $\mu$m was used. By the moment of passage of the next pulse, all information was digitized and stored, thus generating one frame. By the time of arrival of the next electron beam, the detector was prepared to perform measurements and record the next frame.

454
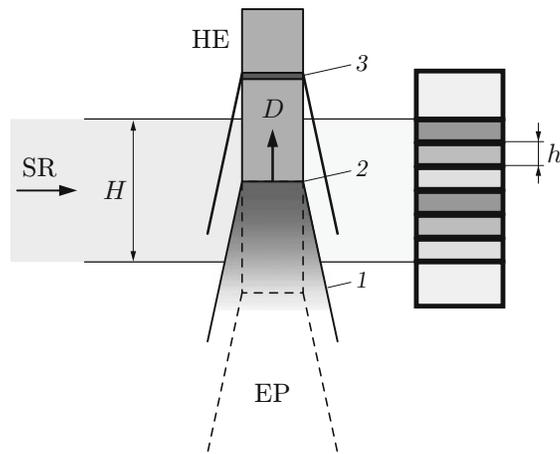
Fig. 2. Schematic of the experimental determination of the density distribution along the charge axis: SR denotes synchrotron radiation beam; EP denotes explosion products; the sequential positions of the front relative to the recording region are denoted as 1, 2, and 3.
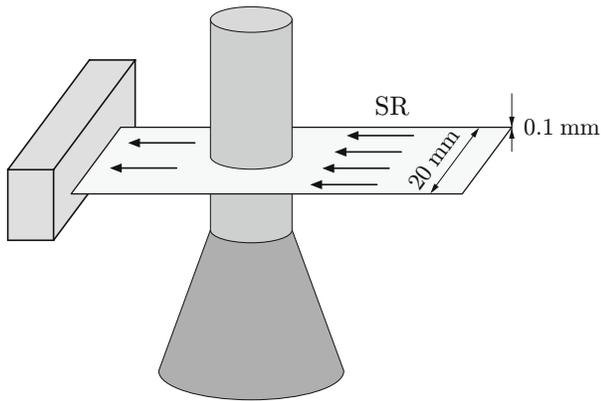


Fig. 3                                                                           Fig. 4

Fig. 3. Schematic of the experiment for obtaining tomographic images in charges of cylindrical shape.
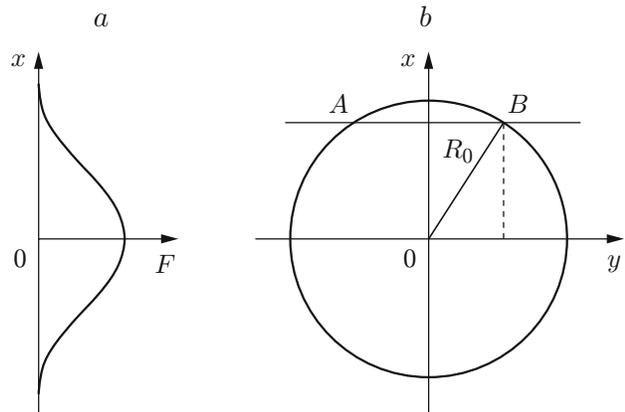
Fig. 4. Schematic of recording of x-ray shade in the calculation of the density distribution in axisymmetric flows: (a) mass distribution on the rays passing through the charge; (b) diagram of the passage of the $AB$ ray through the charge.

Two density recording methods were used. In the first of them, the charge was placed horizontally, and its axis was in the plane of the beam (Fig. 2). In this case, the front of the process, which generally moves at a variable velocity $D$, sequentially passed through positions 1, 2, 3, etc.

In the second method, the beam was directed perpendicularly to the charge axis, making it possible to obtain a tomographic image of the process for cylindrical charges because this provided axial symmetry of the flow of explosion products. A schematic of the experiment is given in Fig. 3.

To determine the mass of the material moving along the beam, the radiation absorption was calibrated by the detector depending on the mass load (or the product of the density and thickness HE $Y = \rho d$ (the quantity $Y$ is in grams per squared centimeter). The degree of attenuation of the transmitted radiation depends only on the integral of the density over the segment occupied by the explosion products (the beam propagates along a straight line). In the corresponding geometry (Fig. 4), from the transmitted radiation density measured by the detector $F(x)$

455
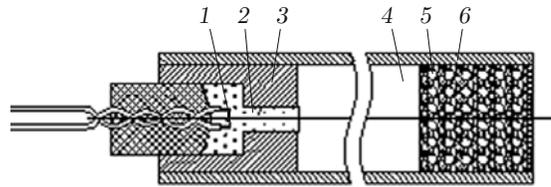
Fig. 5. Experimental assembly used to study the development of detonation transformation by means of SI: 1) electric detonator bridge; 2) additional bulk explosive; 3) generator of initiating stimulus; 4) air gap; 5) passive explosive charge; 6) plastic tube.
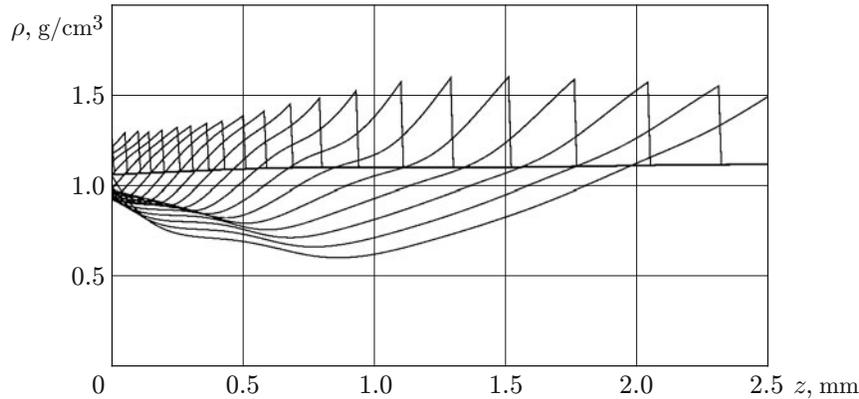


Fig. 6. Experimental density distribution in the PETN powder charge initiated by a shock wave propagating in air.

after the necessary smoothing, the density distribution is found as the radius function [4]:

$$\rho(r) = -\frac{1}{\pi r}\frac{d}{dr}\int\limits_{r}^{R_0}\frac{xF(x)}{\sqrt{x^2 - r^2}}\,dx.$$

**2. Results of Experiments.** A schematic diagram of the experimental investigation of detonation transfer from an active to a passive charge through air is shown in Fig. 5. The passive charge in a thin-walled plastic tube of 16 mm inner diameter was loaded by a shock wave produced in the air gap by detonation of a bulk charge initiated by explosion of a conductor. The shock velocity in the gap was varied by changing the weight of the charge 2 and was measured by contact sensors. The flow parameters behind the shock wave and during its reflection from the target were calculated taking into account dissociation, ionization, and variation in the heat capacity of the gases.

Figure 6 gives experimental curves characterizing the density distribution $\rho$ in the axial section of the PETN charge. The initial density of the explosive was $\rho_0 = 1.1$ g/cm$^3$. The velocity of the direct shock wave was 2.4 km/sec, the pressure behind its front was 8 MPa, and the pressure upon reflection from the hard wall was 60 MPa.

The repetition frequency of electron beams in the accelerator was $f = 2 \cdot 10^6$ sec$^{-1}$; therefore, frames with an exposure of $10^{-9}$ sec followed each 0.5 $\mu$sec, making it possible to determine the velocity $D$ of propagation of the process in the passive charge.

The mass velocity and pressure at the maximum density points were found from known $\rho$ and $D$ by the relations

$$u = D(\rho/\rho_0 - 1), \qquad P = D^2(\rho - \rho_0).$$

The calculation results are given in Fig. 7. From these data, it can be found that the acceleration of the transition regime begins in 1 $\mu$sec after the arrival of the shock wave at the boundary of the charge, whose density at this time increases to $\rho = 1.34$ g/cm$^3$ at $D = 475$ m/sec and $u = 86$ m/sec. The pressure at this point is 45 MPa.

**3. Discussion of the Results.** At present, the following explosive-transformation regimes are known [5] and are used to explain all experimental data on the development of explosion processes:

456
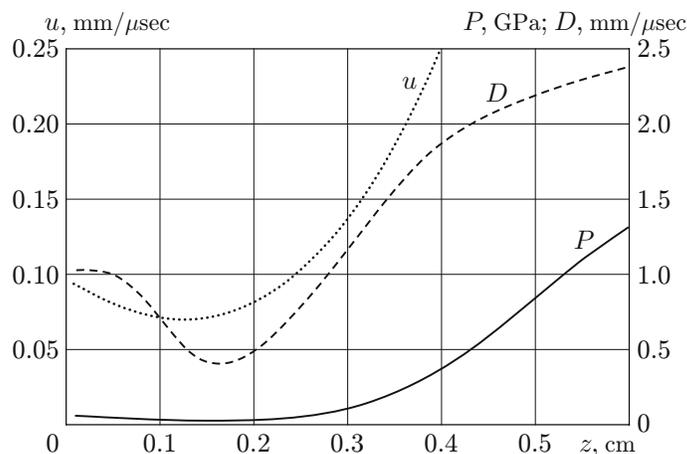
Fig. 7. Experimental curves of the pressure $P$, mass velocity $u$, and velocity of the luminescence front $D$ versus the distance $z$ from the end of the charge.

1. Normal layer-by-layer combustion propagating at a pressure-dependent velocity.

2. Convective combustion — the type of combustion of solid energetic materials having gas-dynamic porosity. Combustion is accomplished by jets of the burned material penetrating into energetic material. Convective combustion occurs upon reaching the pressure of failure of normal combustion $p_{\mathrm{cr}}$ at a certain time $t_*$.

3. Predetonation wave process (low-velocity detonation) which is a wave process with a low degree of decomposition of the material behind the compression wave.

4. Normal detonation.

The pressure determined in the experiments is insufficient to provide the formation of reaction centers due to compression of the explosive. Apparently, the pressure can increase only due to the combustion caused by filtration of hot gases from the region formed on the charge boundary upon shock-wave reflection. We show that the well-studied classical types of combustion [9] cannot provide the pressure level recorded in the experiment.

Let us estimate the density of the gaseous products $\rho_g$ in the region of convective combustion, assuming that the gas is ideal. Then, the density is expressed as

$$\rho_g = \mu P/(RT).$$

Assuming that the molar mass $\mu = 3 \cdot 10^{-2}$ kg/mole and the temperature $T = 3 \cdot 10^3$ K, we obtain $\rho_g = 50.5$ kg/m$^3$.

Let us obtain an upper-bound estimate for the amount of gas formed in the process at the point considered (time interval $\tau = 1$ $\mu$sec and pressure 45 MPa) for the case of layer-by-layer combustion over the entire surface of PETN granules $S = 3 \cdot 10^4$ m$^{-1}$ in unit volume of the explosive. We use the classical concept of convective combustion, according to which combustion occurs at a constant mass velocity $u_m$ at an appropriate pressure; the mass velocity of layer-by-layer combustion depends linearly on the pressure in the region of the products:

$$u_m = \alpha_* P \tag{1}$$

(for PETN, $\alpha_* = 2 \cdot 10^{-6}$ kg/(m$^2 \cdot$sec$\cdot$ Pa) [10]). Under the above assumptions, we obtain $u_m = 90$ kg/(m$^2 \cdot$sec) and $\rho_g = \alpha_* S \tau P = 2.7$ kg/m$^3$.

Since, at the time $t_*$, the porosity of the explosive is almost halved due to compression, the final density of the products can be estimated as 5 kg/m$^3$, which is an order of magnitude smaller than the value obtained in the experiment. Let us also show that within a certain characteristic time, classical layer-by-layer combustion cannot develop. For this, we estimate the width of the heating region that should provide the necessary velocity of layer-by-layer stationary combustion (1) (regime 1). According to [10], the temperature distribution in the charge is given by

$$T = T_0 + (T_k - T_0) \, \mathrm{e}^{-ux/\chi}, \tag{2}$$

where $\chi$ is the thermal diffusivity (for PETN, $\chi = 2 \cdot 10^{-6}$ m$^2$/sec), $T_k$ is the boiling point, and $u$ is the linear burning rate.

457
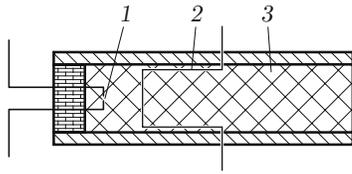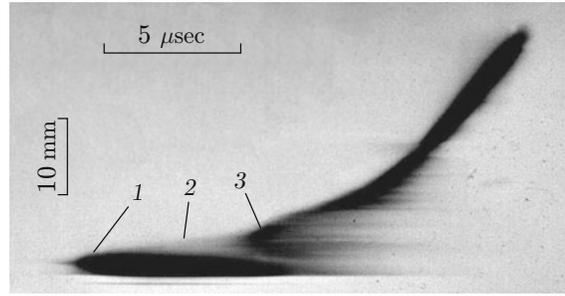
Fig. 8



Fig. 9

Fig. 8. Schematic of measurements of the mass burning rate during spark initiation: 1) spark gap; 2) mass rate sensor foil; 3) PETN charge.

Fig. 9. Streak record of self-luminescence during spark initiation of powder PETN: 1) quasi-stationary initial region; 2) transition regime; 3) detonation.
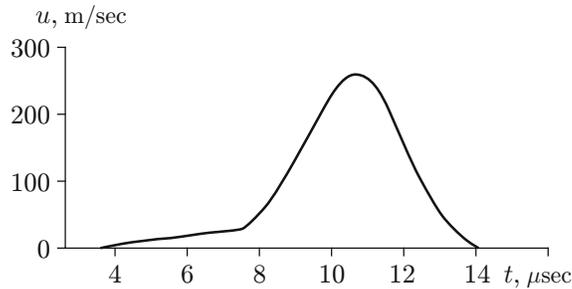


Fig. 10. Mass velocity profile $u$ in a PETN charge powder for spark initiation.

Since $u_m = u\rho_{00}$, for PETN of density $\rho_{00} = 1.8 \cdot 10^3$ kg/m$^3$, we have $u = 5 \cdot 10^{-2}$ m/sec. The characteristic width of the heating region $\delta$ corresponding to this rate is determined, with the use (2), from the relation

$$\frac{u}{\chi}\delta = 1$$

and is $4 \cdot 10^{-5}$ m.

Let us estimate the heating-region width that can occur in the explosive if its boundary is exposed to a heat source maintaining a constant temperature $T_k$ on it for the maximum admissible time $\tau$. In the process studied, the maximum time $\tau$ cannot exceed $10^{-6}$ sec; therefore, $\delta = \sqrt{\chi\tau} = \sqrt{2 \cdot 10^{-12}}$ m $= 1.4 \cdot 10^{-6}$ m. The obtained value is an order of magnitude smaller that for combustion of energetic material in accordance with law (1).

The above estimates unambiguously indicate that the classical combustion law cannot be used to treat the obtained results.

Let us show that the regime considered above has characteristics similar to those of high-velocity convective combustion of secondary powder explosives initiated by a pulsed spark discharge and overdriven gaseous detonation [11–15].

In the experiments described in [11, 12], a PETN powder charge (Fig. 8) identical to that used above (see Fig. 5) was placed in a Plexiglas tube with an inner diameter of 5 mm and a wall thickness of 1 mm. A streak photo record of the process initiated by a spark discharge is given in Fig. 9. It shows the occurrence of a quasi-stationary luminescence region near the discharge. After 3–4 $\mu$sec, a transition regime transforming to detonation propagates from this region with a velocity of 800 m/sec.

The mass velocity profile at a distance of 5 mm from the spark gap measured with a foil sensor is given in Fig. 10. The sensor records the following stages of the process:

1. In 4 $\mu$sec after the discharge, the foil begins to move with a constant acceleration and by the time $t = 7.5$ $\mu$sec, it is accelerated to a velocity approximately equal to 20 m/sec.

458
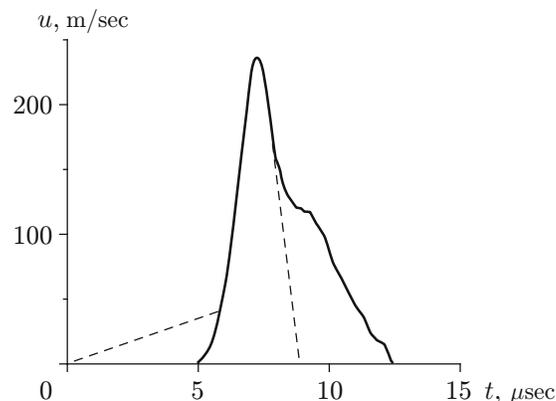
Fig. 11. Mass velocity profiles for initiation by a spark (dashed curve) and overdriven detonation (solid curve).

2. At $t = 7.5$ $\mu$sec, an inflection appears in the velocity profile, indicating an abrupt change in the acceleration and, hence, in pressure.

3. At $t = 7.5$–$11.0$ $\mu$sec, the value of $u$ increases almost linearly to $u = 240$ m/sec, and then decreases due to fracture of the shell and unloading.

Consequently, at the maximum velocity, the pressure is approximately 1.7 GPa, i.e., much higher than at the same velocity $D$ in experiments with initiation of the charge by an air shock wave, in which $u = 120$ m/sec and $P = 1.06$ GPa. However, during spark initiation, at the point of inflection of the mass velocity profile, involving a sharp acceleration of gas release, there is a different situation: $u = 20$ m/sec and $P = 0.15$ GPa.

The difference between the experimental data obtained during shock-wave and spark initiation is due to the large difference in charge diameter between the experiments compared. Decreasing the charge diameter in the x-ray technique is now impossible because this will reduce the accuracy of the synchrotron diagnostics.

A PETN powder charge of 6 mm diameter is initiated with a nearly 50% probability by overdriven gaseous detonation produced by the entry of ordinary gaseous detonation into a cone if the pressure behind the detonation front is $P = 5.2$ MPa (accordingly, for reflection from a hard wall, $P = 23$ MPa) [14]. The kinematics of self-luminescence in the regime occurring in the explosive corresponds to Fig. 9. Figure 11 gives experimental mass velocity profiles obtained during spark and gaseous detonation initiation [15]. In view of the shift in time, the curves almost coincide, except in the region corresponding to the time of propagation of the precursor, i.e., the processes are identical in the two cases.

In [13], the regime corresponding to region 2 in Fig. 9 was calculated for a one-dimensional model of a multivelocity two-phase medium. Satisfactory agreement with the experimental data was achieved only when the mass burning rate was ten times the classical mass velocity. These calculations confirm the validity of the above estimates. In a two-dimensional formulation taking into account the effect of expansion in charges with a low-strength shell, the gasification rate necessary for the existence of the regime considered is even higher.

In a calculation for the two-dimensional model of a multivelocity heterogeneous medium postulating the classical combustion law, transition from combustion to detonation was obtained only for charges of a low-density disperse explosive confined in a steel shell having considerable strength [16]. This calculation did not yield the regime whose parameters correspond to the data presented in Fig. 7. At the same time, its results agree with the experimental regularities of propagation of waves of ordinary convective combustion and nonideal detonation [17–19].

The aforesaid suggests that for the initiation of a powder HE by a shock wave produced by an active charge in air and for spark and gaseous-detonation initiation, the determining stage of the detonation process is the occurrence of high-velocity convective combustion whose mechanism cannot be explained using the conventional combustion concepts. The first experimental results indicating the existence of this regime were obtained in [1]. The essence of this regime is that, with the usual conditions satisfied (increasing charge diameter), its occurrence guarantees the development of detonation transformation up to the final stages. Among all known regimes, only shock-wave initiation have such properties.

459
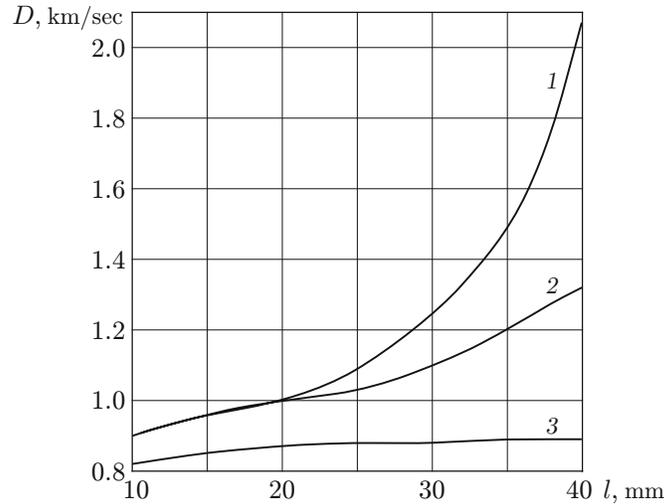
Fig. 12. Velocity $D$ of the transition regime versus distance traveled by the wave during propagation in a thin-walled Plexiglas tube for charge diameters $d = 5$ (1), 4 (2), and 3 mm (3).

The high-velocity convective combustion considered here has another property characteristic only of the process behind a shock wave. Figure 12 gives the results of investigation of the kinematics of the transition regime occurring during spark initiation of bulk PETN [13]. The bulk PETN charge was placed in Plexiglas tubes of various diameters with 1 mm thick walls. In all cases, in the initial stage there was high-velocity convective combustion which was not initiated by the compression wave.

In charges of $d \geq 4$ mm diameter, the velocity of the transition regime increased until ordinary detonation regimes occurred. For $d = 3$ mm at a distance of about 20 mm from the initiating gap, the velocity $D$ reached the limiting value $D = 830$ m/sec and ceased to increase. This value remained unchanged throughout the recording region, i.e., at a distance along the charge equal to not less than seven charge diameters. Obviously, the value of $D$ will remain constant even for greater charge length. There is reason to believe that it is possible to choose the least diameter $d_{cr}^*$ of a charge without a shell (in practice, with a shell of very low strength) for which the high-velocity convective combustion regime can propagate any distances. As shown in [11], with transition of this process into a charge of the same HE with $d > d_{cr}^*$, the velocity of the wave increases up to the moment of transition to normal detonation. The critical diameter of the region of ordinary detonation $d_{cr}$ is determined as the minimum diameter of the explosive charge which can still provide steady-state propagation of self-sustained detonation, i.e., a hypersonic stationary complex consisting of a shock wave followed by chemical reaction [5]. Thus, the diameter $d_{cr}^*$, similarly to the critical diameter of ordinary detonation $d_{cr}$, determines the limiting conditions of high-velocity convective combustion, whose propagation mechanism is not completely understood (it is obviously not a shock-wave one). Following [18–20], we will call such high-velocity combustion ablation combustion.

The existence of ablation combustion having a critical diameter changes the established concepts of the mechanism of initiation of powder explosives by a powerful external action with low energy. We note that this issue is not discussed in the last edition of the Physics of Explosion [5], but in the previous edition of 1975 [21], the development of detonation during spark discharge is treated as follows. Extremely high energy concentration is attained in the channel. A sharp rise in temperature and, hence, pressure leads to the formation of a shock wave in the explosive charge, which expands from the plasma channel. The shock wave and strong heating of the explosive provide initiation and propagation of the explosive transformation process. In practice, the critical initiation conditions hold already during the occurrence of ablation combustion. Shock-wave initiation can take place in the next stage of evolution of high-velocity ablation combustion but the critical initiation conditions occur earlier.

460

**4. On the Mechanism of High-Velocity Combustion.** A possible mechanism involved in the acceleration of combustion is considered in [13, 22]. In [13], the necessary combustion velocity was obtained under the assumption that on the surface of a particle in hot gas flow, a layer of vaporized material forms in which waves destroyed by the flow arise. The conditions of initiation of this regime, i.e., the specific ignition conditions were not analyzed in [13].

In [22], the integral acceleration of the regression of the condensed phase is explained by crushing of explosive granules in the compression wave, leading to a considerable increase in the burning surface area which then follows the usual law. However, as shown above, the time is not sufficient to form a heating region that provides the classical type of combustion.

The specific ignition conditions were studied experimentally in great detail in [20] using multibeam pyrometry. This made it possible to measure the ignition delay of dispersed PETN particles in a gas detonation wave. It was shown that during the delay time, a molten layer about 1 $\mu$m thick was formed on a particle surface, which was destroyed by wave perturbations in the high-velocity flow. This led to a rapid discharge of the molten particles into the region of hot products, resulting in an order of magnitude increase in the integral burning rate. The validity of the obtained results is supported by the fact that in smokeless pyroxylin powders which do not melt, high-velocity combustion does no occur.

At present, however, there is no adequate model for describing all features of development of the high-velocity combustion regime, which is important for practical application and determination of conditions of safe handling of explosives. This may be due to the fact that available models use incorrect initial conditions, for example, the notion of ignition temperature, which is absent in both solid-phase and gas-phase ignition theories; in addition, regardless of the characteristic time of the process, the validity of the classical pressure dependence of the burning rate, given by formula (1) is postulated.

## REFERENCES

1. A. F. Belyaev, M. A. Sadovskij, and I. I. Tamm, "Application of the similarity law in explosions to transmission of detonation," *J. Appl. Mech. Tech. Phys.*, No. 1, 3–17 (1960).

2. K. A. Ten, O. V. Evdokov, I. L. Zhogin, et al., "Density distribution at the detonation front of cylindrical charges of small diameter," *Combust., Expl., Shock, Waves.*, **43**, No. 2, 204–211 (2007).

3. O. V. Evdokov, A. N. Kozyrev, V. V. Litvinenko, et al., "High-speed x-ray transmission tomography for detonation investigation," *Nucl. Instrum. Methods Phys. Res. Sec. A.*, **575**, Nos. 1/2, 116–120 (2007).

4. K. A. Ten, V. M. Aulchenko, O. V. Evdokov, et al., "Measuring density distribution during detonation of explosive using synchrotron radiation," in: *Physics of Extreme States of Materials*, Inst. of Problems of Chem. Phys., Russian Acad. of Sci., Chernogolovka (2003), pp. 40–42.

5. L. P. Orlenko (ed.), *Physics of Explosion* [in Russian], Vol. 1, Fizmatlit, Moscow (2004).

6. V. M. Aulchenko, O. V. Evdokov, L. I. Shekhtman, et al., "Current status and further improvements of the detector for imaging of explosions," *Nucl. Instrum. Methods Phys. Res., Sec. A.*, **603**, Nos. 1/2, 73–75 (2009).

7. V. Aulchenko, V. Zhulanov, L. Shekhtman, et al., "One-dimensional detector for study of detonation processes with synchrotron radiation beam," *Nucl. Instrum. Methods Phys. Res., Sec. A*, **543**, No. 1, 350–356 (2005).

8. V. Aulchenko, O. Evdokov, S. Ponomarev, et al., "Development of fast one-dimensional x-ray detector for imaging of explosions," *Nucl. Instrum. Methods Phys. Res. Sec. A*, **513**, No. 1/2, 388–393 (2003).

9. A. F. Belyaev, V. K. Bobolev, A. I. Korotkov, A. A. Sulimov, and S. V. Chuikov, *Transition from Combustion of Condensed Systems to Explosion* [in Russian], Nauka, Moscow (1973).

10. K. K. Andreev and A. F. Belyaev, *Theory of Explosives* [in Russian], Oborongiz, Moscow (1960).

11. V. V. Andreev, P. I. Zubkov, G. I. Kiselev, and L. A. Luk'yanchikov, "One detonation regime of powder explosives of low density," in: *Dynamics of Continuous Media* (collected scientific papers) [in Russian], No. 10, Inst. of Hydrodynamics, Sib. Div., Russian Acad. of Sci., Novosibirsk (1972), pp. 183–188.

12. V. V. Andreev and L. A. Luk'yanchikov, "Low-speed detonation mechanism in PETN powder with spark initiation," *Combust., Expl., Shock Waves.*, **10**, No. 6, 818–823 (1974).

13. V. V. Andreev, A. P. Ershov, and L. A. Luk'yanchikov, "Two-phase low-speed detonation of a porous explosive," *Combust., Expl., Shock Waves*, **20**, No. 3, 330–334 (1984).

14. V. V. Grigor'ev, L. A. Luk'yanchikov, É. R. Pruuél, and A. A. Vasil'ev, "Initiation of a porous explosive by overdriven gas detonation products," *Combust., Expl., Shock Waves*, **37**, No. 5, 572–579 (2001).

15. L. A. Luk'yanchikov, "Initiation systems using secondary explosives," *J. Appl. Mech. Tech. Phys.*, **41**, No. 5, 806–817 (2000).

16. O. A. Dibrov, S. V. Tsikin, and Yu. V. Yanilkin, "Two-dimensional numerical simulation of deflagration-to-detonation transition for a porous explosive using a model of a multivelocity heterogeneous medium," *Combust., Expl., Shock Waves*, **36**, No. 3, 374–383 (2000).

17. A. A. Sulimov, V. S. Ermolaev, A. I. Korotkov, et al., "Laws of propagation of convective combustion waves in a closed volume," *Combust., Expl., Shock Waves*, **23**, No. 6, 669–675 (1987).

18. V. A. Ashchepkov and V. V. Sten'gach, "Predetonation section of the combustion-detonation transition in PETN," *Combust., Expl., Shock Waves*, **10**, No. 6, 783–786 (1974).

19. A. A. Sulimov and B. S. Ermolaev, "Quasi-stationary combustion in energetic materials with low porosity," *Khim. Fiz.*, **16**, No. 9, 51–72 (1997).

20. V. V. Grigor'ev, L. A. Luk'yanchikov, and É. R. Pruuél, "Ignition of PETN particles by a gas detonation wave," *Combust., Expl., Shock Waves*, **33**, No. 2, 238–242 (1997).

21. K. P. Stanyukovich (ed.), *Physics of Explosion* [in Russian], Nauka, Moscow (1975).

22. A. P. Ershov, "Modeling of the deflagration to detonation transition in porous PETN," in: *Proc. of the 11th Int. Symp. on Detonation* (Snowmass Village, 1998), Ampersand Publ. Group (2000), pp. 686–692.